

Article

# Investigation of the Pitch Load of Large-Scale Wind Turbines Using Field SCADA Data

Fan Zhang <sup>1,\*</sup>, Juchuan Dai <sup>2,\*</sup>, Deshun Liu <sup>2</sup>, Linxing Li <sup>2</sup> and Xin Long <sup>3</sup>

<sup>1</sup> College of Mechanical and Electrical Engineering, Central South University, Changsha 410083, China

<sup>2</sup> School of Mechanical Engineering, Hunan University of Science and Technology, Xiangtan 411201, China; liudeshun@hnust.edu.cn (D.L.); lilinxin2018@163.com (L.L.)

<sup>3</sup> XEMC Windpower Co., Ltd., Xiangtan 411000, China; longxin\_XEMC@163.com

\* Correspondence: zhangfan730@csu.edu.cn (F.Z.); juchuandai@163.com (J.D.); Tel.: +86-1587-326-5266 (F.Z.)

Received: 20 December 2018; Accepted: 31 January 2019; Published: 5 February 2019



**Abstract:** Variable pitch technology is an indispensable key technology of large-scale wind turbines. The reliable pitch mechanism is the basic guarantee for achieving variable pitch. At present, the main problem with the design and maintenance of the variable pitch mechanism is that the pitch load is not clearly known. This paper focuses on obtaining pitch load characteristics through extracting SCADA (Supervisory Control and Data Acquisition) data. Here, the pitch load refers to the resistance moment to be overcome when the wind turbine blade is rotated on its own axis. From the data collected by the SCADA system, although the edgewise moment and the flapwise moment cannot be obtained, the pitch torque (load) can be extracted indirectly. This provides data support for the research. Specifically, the pitch moment is obtained by indirect calculation of the pitch motor current. Then, the effects of the wind speed, rotor speed, hub angle and pitch angle on the pitch load are theoretically analyzed. To obtain more reliable results, data preprocessing algorithms are presented to consider the data filtering range, the elimination of abnormal values and data dispersity. Subsequently, the influence mechanisms of wind speed, rotor speed, hub angle and pitch angle on the pitch load are investigated in detail based on the SCADA data.

**Keywords:** wind turbines; SCADA data; pitch load; load characteristics

## 1. Introduction

In recent years, the world wind power industry has developed rapidly. By the end of 2017, the total installed capacity of the global wind power had reached 539.1 GW [1,2]. With the rapid development of the wind power industry, the unit capacity of wind turbines has also been on the rise, and the installed locations are moving to more distant land and sea areas. Therefore, higher requirements for the reliability of wind turbines are put forward. As one of the key technologies of large-scale wind turbines, pitch-control has been widely applied. It can control the output power of the wind turbine and ensure the safe and stable operation of the wind turbine by changing the pitch angle to control the capture of wind energy [3–5]. At the same time, the pitch system bears a very complex aerodynamic forces due to the mean and turbulence flow field and wind shear, rotation and gravity. As a result, the pitch system becomes a component with a high fault rate in wind turbines [6,7]. Once a fault or abnormality of the pitch system occurs, it is likely to cause serious accidents, such as pitch bearing cracking, blade rupture, or tower collapses.

To date, there is still a lack of sufficient understanding of the variable pitch load of wind turbines, for several reasons. The first is that there are several factors that affect the pitch load. The second is that the pitch load of large-scale wind turbines is difficult to simulate accurately in the laboratory. Third, it is difficult to directly measure the pitch load of large-scale wind turbines in wind farms.

Nevertheless, research of the pitch load has always been the focus of attention. Many methods, such as the blade element momentum theory [8–10], dynamic stall model [11,12], computational fluid dynamics [13–15] and wind tunnel experimental research [16,17], have been employed to investigate the aerodynamic characteristics of wind turbine blades, which is one of the main factors of the pitch load. For example, by combining the element momentum theory with the dynamic stalling model, a deep theoretical analysis of the pitch load characteristics of a megawatt-scale wind turbine was carried out. In addition, a calculation method was put forward to investigate the pitch load that was induced by centrifugal force, aerodynamic force and gravity [18,19]. In addition, the driving motor model, three-stage planetary gear reducer model and transmission shaft model were established to investigate the dynamic response behaviors of the pitch system under pitch load [20]. Furthermore, the flexible deformation of the blade was considered to investigate the blade load and dynamic characteristics more accurately [21]. The pitch behavior of wind turbines in consideration of wind turbulence was analyzed [22]. Moreover, the wind turbine performance was optimized by measuring bending moments of individual blades of the wind turbine and using independent pitch control strategies [23]. On the other hand, the massive SCADA (supervisory control and data acquisition system) data of wind farms provides a new method of wind turbine performance analysis. For instance, based on SCADA data, condition monitoring of wind turbines [24–27], output power investigating of wind turbines [28–30], assessment of wind resource characteristics [31] and wind power coefficient analysis [32] were carried out. However, less work involves the investigation of wind turbine pitch load by using field SCADA data. Thus, it is quite meaningful to fill this knowledge gap by investigating the pitch load of large-scale wind turbines based on SCADA data.

The remaining part is organized as follows. In Section 2, the influences of aerodynamic force, centrifugal force, gravitational force and inertial force on the pitch load were theoretically analyzed. In Section 3, the pitch torque (load) of the blade around its own axis was obtained indirectly by extracting the relevant state parameters of the pitch load from the SCADA data. Considering the influence of the external disturbance on the sensing system, SCADA data contains a certain amount of null value and zero value, which will affect the data validity. Thus, a data extraction and preprocessing method is presented in Section 4. Moreover, using the kernel density estimation (KDE) method, data reliability processing is carried out. The influencing mechanism of wind speed, rotor speed, hub angle, and pitch angle on the pitch load is also investigated in Section 4. Finally, Section 5 ends the paper by summarizing the main conclusions.

## 2. Influencing Factors of Pitch Load—Theoretical Analysis

In this section, the influence factors of pitch load will be analyzed theoretically, which is beneficial to grasp the basic characteristics of pitch load from the macro point of view and to provide guidance for the investigation of the SCADA data of pitch load. During the operation of a wind turbine, there are many factors that affect the pitch load. Specifically, it is not only affected by the external wind speed but also by the properties of the blade, such as the blade weight, structure (layout of pitch axis, center of gravity, aerodynamic center). In our earlier work, the theoretical analysis of the variable pitch load was basically completed. For example, in [18], the pitch load model caused by aerodynamic force, centrifugal force and gravity were each established. In addition, the inertial force around the pitch axis that is generated during blade pitching will also affect the pitch load. For wind turbines with a certain structure, the pitch load acting on the blade element can be obtained by adding the four forces without considering the coupling effects between the loads. That is:

$$\begin{cases} dT_p = dT_Z + dT_C + dT_G + dT_I \\ dT_Z = f_Z(v, \omega, \beta) \\ dT_C = f_C(\omega) \\ dT_G = f_G(\varphi) \\ dT_I = f_I(d^2\beta/dt^2) \end{cases} \quad (1)$$

where  $dT_p$  is the pitch load acting on a section (element) of the blade;  $dT_Z$  is the pitch load component induced by aerodynamic force on a section of the blade;  $dT_C$  is the pitch load component induced by centrifugal force on a section of the blade;  $dT_G$  is the pitch load component induced by gravity on a section of the blade;  $dT_I$  is the pitch load component induced by the inertial force on a section of the blade;  $\beta$  is the blade pitch angle;  $\omega$  is the rotor speed; and  $\varphi$  is the hub angle.

The general relation model between pitch load and related operation parameters is given in Equation (1). To simplify the explanation, the general expression between the pitch load and the related parameters is given in the equation, but the very specific physical expression is not given. The reason is that relevant research has been found in many references (for example, in [18,19,21]), and the emphasis of this section is to clarify the factors affecting the pitch load and to provide the basis for a subsequent SCADA data investigation. In the remainder of this section, the relationship between pitch load and related parameters will be further explained.

It is worth noting that only four parameters, wind speed, rotor speed, pitch angle and hub angle, appear in Equation (1). They are all variables. Due to the time-varying characteristics of wind speed, it is always a variable in Equation (1). The change of wind speed will lead to the corresponding control of rotor speed, so rotor speed is a variable. At the same time, the blade pitch angle will vary according to the operating conditions. Due to the rotation of the wind rotor, the hub angle is also variable.

More specifically, for wind turbines with a certain structure, the aerodynamic component is expressed as a dependent variable that is related to wind speed, rotor speed and pitch angle. In other words, any change in each of the three variables will bring about a change in the aerodynamic component of the pitch load. From the basic principles of mechanics, the centrifugal force component is mainly related to the rotor speed. The gravity component is mainly related to the hub angle. The inertial force component is related to pitch acceleration. It can be seen that the influence of the above variables on the pitch load should be considered when investigating the SCADA data. It should be noted, however, that the effect of the inertial force is not taken into account in the subsequent analysis. There are two reasons: (1) the inertial force exists only when the pitch rate is in the acceleration and deceleration state but does not exist when the pitch rate is invariant; (2) the sampling rate of SCADA data is not suitable for micro-scale dynamic characteristic analysis. The relationship between the pitch load and the aforementioned factors is shown in Figure 1.

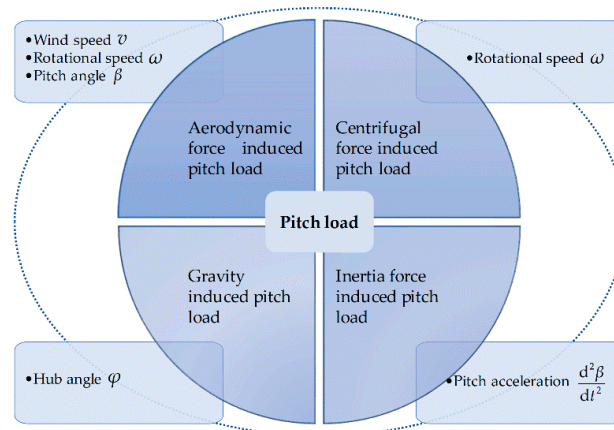


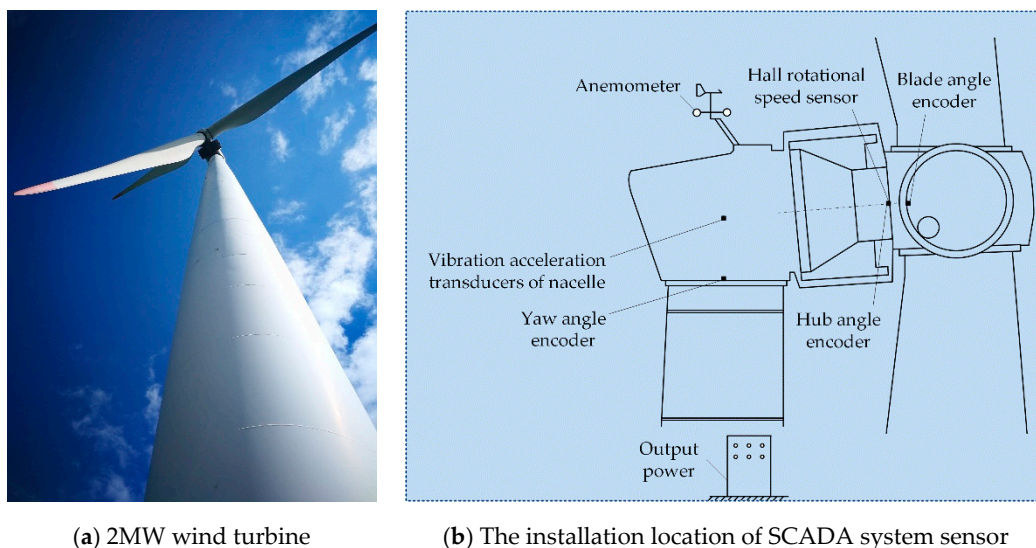
Figure 1. Influence factors of pitch load.

### 3. Data Extraction of the Blade Pitch Load

#### 3.1. Introduction of SCADA Data

To investigate the pitch load, a 2 MW PMSG direct-driven wind turbine, which has a SCADA system, was selected. The wind turbine contains independent pitch mechanism and adopts active variable pitch control strategy. Figure 2a shows the 2 MW wind turbine investigated in the paper.

Figure 2b shows the installation location of the SCADA system sensor. The wind speed is measured by an anemometer mounted on top of the nacelle. The rotational speed is measured by Hall rotational speed sensor mounted on the nacelle near the main shaft. The hub angle is measured by the hub angle encoder mounted on the nacelle near the main shaft. The pitch angle is measured by the blade angle encoder mounted on the wind rotor near the pitch bearing. The parameters of the wind turbine are shown in Table 1. The SCADA system collects and stores operating parameters of the wind turbine with a time interval of 1 second (sampling frequency is 1 Hz). Table 2 shows the parameter name and the raw data style of the SCADA system. It can be seen that those parameters include wind speed, rotor speed, hub angle, current of pitch motor, blade pitch angle, output power, and so on. However, the pitch torque (load) of the blade around its own axis, which is the key parameter for understanding the load acting on the blade, was not collected. The reason for not collecting the pitch torque (load) is that there was no suitable sensor for the torque (load) to measure at the blade root. The advantage of the SCADA system is to store the operating parameters of the wind turbine continuously, which provides a big data foundation for the research of this paper.



(a) 2MW wind turbine

(b) The installation location of SCADA system sensor

Figure 2. 2MW wind turbine and installation location of the SCADA system sensor.

Table 1. Main technical parameters of the wind turbine.

Parameters	Value
Rated output power (W)	$2 \times 10^6$
Cut-in speed (m/s)	3
Rated wind speed (m/s)	11
Rated power of pitch motor (W)	9800
Rated armature current of pitch motor (A)	38
Reduction ratio (from pitch motor to blade root)	1954.6

Table 2. Raw data style collected by the SCADA system.

Time (h:m:s)	Wind Speed (m/s)	Hub Angle (rad)	Rotor Speed (rad/s)	Current of Pitch Motor 1 (A)	Current of Pitch Motor 2 (A)	Current of Pitch Motor 3 (A)	Angle of Blade 1 (rad)	Angle of Blade 2 (rad)	Angle of Blade 3 (rad)	Output Power (W)
14:20:01	3.5	2.03	0.78	7.78	7.72	5.38	0.00	0.00	0.00	126,000
14:20:02	3.7	2.82	0.79	8.64	5.9	5.46	0.00	0.00	0.00	133,000
14:20:03	3.8	3.60	0.79	8.46	5.74	6.16	0.00	0.00	0.00	132,000
...	...	...	...	...	...	...	...	...	...	...
18:39:01	6.2	4.13	1.37	12	12.54	10.36	0.00	0.00	0.00	737,000

### 3.2. Calculation of the Pitch Load

Since the pitch load is not directly given in the SCADA system, indirect calculation of the pitch load through other parameters is the basis of subsequent analyses and is also the work to be done in this section. One thing that needs to be explained is that the pitch load investigated here does not include the edgewise moment or the flapwise moment. From the data collected by the SCADA system, although the edgewise moment and the flapwise moment cannot be obtained, the pitch torque (load) can be extracted indirectly. The power source of the blade variable pitch is the pitch motor. Therefore, the current of the pitch motor is one-to-one corresponding to the blade pitch load. The SCADA data include the current of the pitch motor. In combination with some parameters of the pitch motor, the electromagnetic torque of the pitch motor can be calculated. This moment acts on the blade through the reducer and is balanced with the blade pitch load. In other words, the pitch load on the blade can be deduced from the current of the pitch motor.

Figure 3 shows the structure of the pitch system of the investigated wind turbine. A blade pitching unit generally include pitch controller, servo drive, servo motor, three-stage planetary reducer, pitch bearing, angle limit switches, battery, power supply, and so on. The power source is a DC (Direct Current) servo motor, and it is connected to the pitch drive gear through a three-stage planetary reducer. When the pitch controller sends a pitch control command, the output torque of the pitch motor passes through the transmission shaft and the three-stage planetary reducer, and finally is transmitted to the root ring of the blade root. Then, the blade rotates with the inner gear ring to change the blade pitch angle.

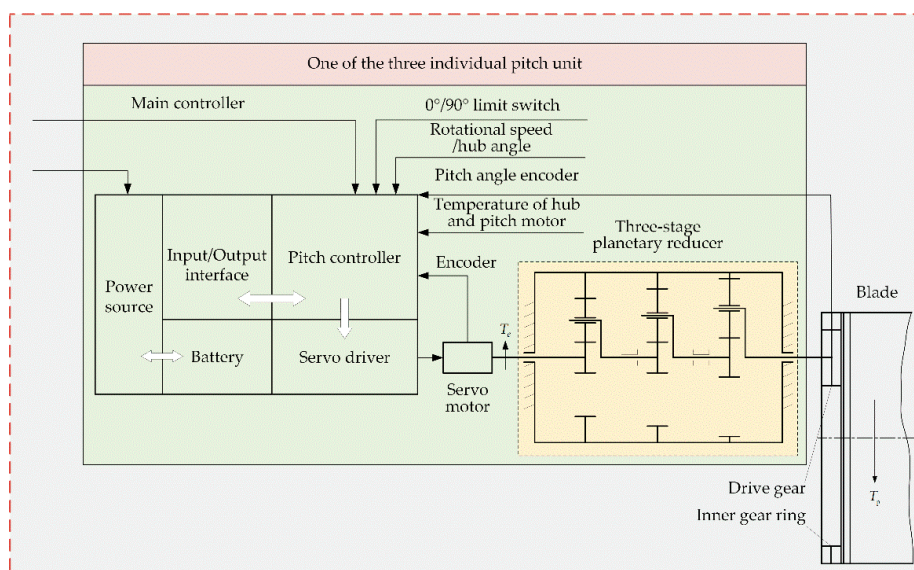


Figure 3. Structural model of the electric pitch system [33].

Ignoring the no-load torque of the DC pitch motor, the output drive torque of the pitch motor can be calculated as:

$$T_e = C_T \Phi I_a \quad (2)$$

where  $I_a$  is the pitch motor current, which can be obtained from the SCADA data;  $\Phi$  is the air gap flux; and  $C_T$  is the torque coefficient.

If the reduction ratio from the pitch motor to the blade root is  $i$ , the pitch load acting on the blade is balanced with the pitch motor output torque, which is:

$$T_p = i\eta T_e \quad (3)$$

where  $\eta$  is the mechanical transfer efficiency of the pitch system.

It should be noted that, as an approximate calculation, the mechanical transfer efficiency in Equation (3) is calculated by 100%. In another scenario, this approximate calculation also does not consider the influence of the blade rotation inertia. It is clear that the inertia force does not affect the blade when the pitch rate remains constant. However, when the pitch rate changes, there is a certain deviation when ignoring the influence of the inertial force. In fact, due to the limitation of the maximum pitch acceleration, neglecting the effect of the inertial force will not cause a large error. From this scenario, the result of the indirect calculation of the pitch load can be used in the subsequent investigation. After the calculation is completed, the pitch load can be added to the SCADA data set. So far, the data preparation is basically completed.

### 3.3. Preprocessing of SCADA Data

Normally, the running parameters that are collected in the SCADA system include normal running data, as well as downtime data, null value and zero value data. The main reason for the null value and zero value appearing is the influence of external disturbances on the sensing system. For example, four parameter curves, including wind speed, rotor speed, hub angle and pitch angle, are shown in Figure 4. Obviously, abnormal data should be eliminated during the analysis process, and normal useful data should be retained. From Figure 4, it can also be seen that the data characteristics of different parameters are not the same. Wind speed is the input of the wind power system and is a random variable. It is not affected by the system control strategy. As shown in Figure 4, wind speed has a random disturbance characteristic with a base value. Rotor speed is the result of the system control and is closely related to the change of wind speed. In other words, its overall trend of change is directly affected by the wind speed. The hub angle curve reflects the real-time running characteristics of the wind rotor and is equivalent to the integral rotor speed, which shows a periodic feature in the figure. The blade pitch angle directly affects the wind energy capture characteristic, which is also affected by the wind speed.

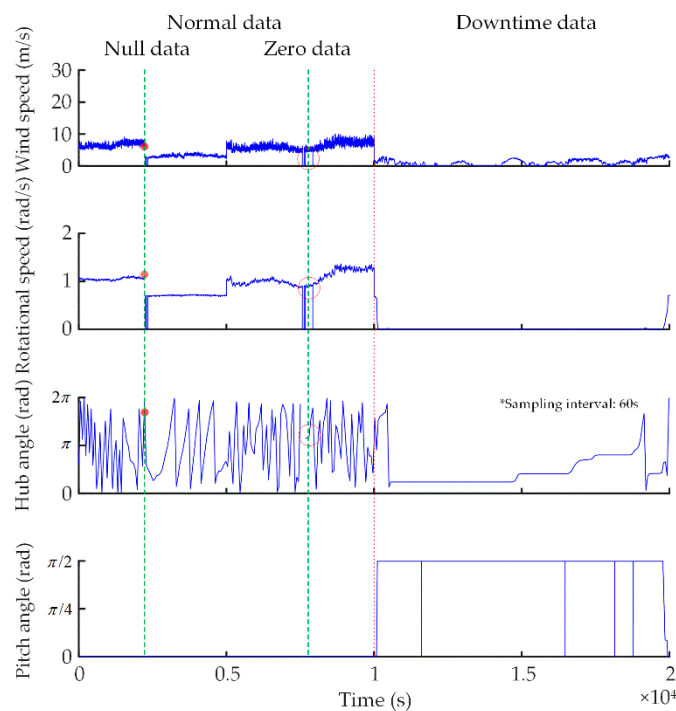


Figure 4. Parameter trends with time.

As stated in the theoretical analysis, not all of the running parameters are needed to investigate the pitch load. Therefore, only the related parameters will be extracted. Thus, the steps of data preprocessing are as follows:

*Step 1:* Extract the data of wind speed, rotor speed, hub angle, output power, pitch angle and pitch motor current. The characters of  $v$ ,  $\omega$ ,  $\varphi$ ,  $P$ ,  $\beta$  and  $I$  are employed to denote these parameters with units of m/s, rad/s, rad, W, rad and A, respectively.

*Step 2:* Eliminate the shutdown data and zero value data by judging the values of  $\omega$  and  $P$ . If  $\omega \leq 0$  or  $P \leq 0$  hold, the corresponding state parameters should be eliminated. Furthermore, null data should also be eliminated.

*Step 3:* Calculate the pitch torque (load)  $T_P$  by using Equation (3). Then, a new SCADA data set, including wind speed, rotor speed, hub angle, pitch angle and pitch load, is constructed.

Using the new SCADA data set, scattering the diagram between different parameters can be easily constructed. For example, Figure 5 gives the scatter diagram of the wind speed and the pitch load. Some interesting phenomena can also be observed from the figure. When the wind speed is greater than approximately 8 m/s, the scatter diagram between the wind speed and the pitch load is more scattered. By examining the details of more parameters, it was found that when the wind speed is greater than 8 m/s and the rotor speed is greater than 1.2 rad/s, the pitch angle is greater than 0 rad, which means that the pitch mechanism is already in the station of motion. It should be noted that since the anemometer was installed on the nacelle behind the wind turbine, the measured wind speed is smaller than the actual wind speed. Thus, although the wind turbine has a rated wind speed of 11 m/s, it may be in a variable pitch state when the indicated wind turbine is below 11 m/s. On the other hand, even if the wind speed does not reach the rated wind speed, the effect of the wind rotor inertia may cause the pitch system to be in a working state.

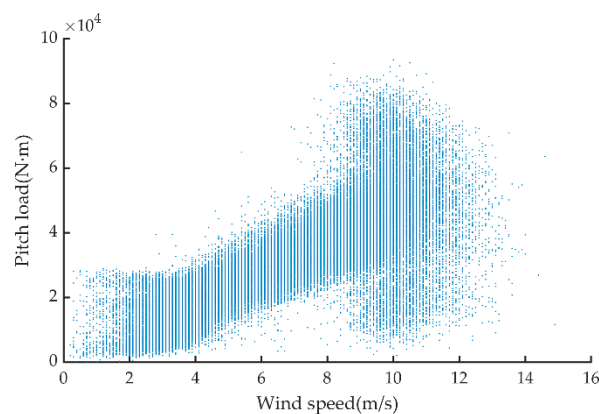


**Figure 5.** Scatter diagram of the wind speed and the pitch load.

#### 4. Investigation of the Pitch Load Based on SCADA Data

As mentioned in the previous section, the main factors affecting the pitch load of the wind turbine are wind speed, rotor speed, hub angle and pitch angle. The pitch angle is a special factor. If the pitch angle is greater than 0 rad, it means that the pitch mechanism has been started, that is, the wind turbine has been operating in the constant power operation state. The variation of the pitch load during this period becomes very complicated; therefore, when investigating the influence of wind speed, rotor speed and hub angle on the pitch load, the data samples with the pitch angle of 0 rad were selected. To understand the influence of each factor on the pitch load from a data point of view, this section will carry out the data investigation.

##### 4.1. Investigation of Wind Speed on the Pitch Load

When investigating the influence of wind speed on the pitch load, the rotor speed and hub angle took a relatively definite value. The sample data extraction was performed as follows:

*Step 1:* Eliminate the data of the wind turbine in a pitch state by judging whether  $\beta = 0$ .

*Step 2:* Select the rotor speed of 0.9 rad/s, 1.0 rad/s, 1.1 rad/s, 1.2 rad/s, with a variation range of  $\pm 0.05$  rad/s. The rotor speed level was determined to set aside the influence caused by operating the pitch mechanism.

*Step 3:* Extract the SCADA data corresponding to the hub angle of 0 rad,  $0.5\pi$  rad,  $\pi$  rad, and  $1.5\pi$  rad under different rotor speeds. The extracted hub angle data have a variation range of  $\pm 0.1$  rad.

The determination of the factor interval requires a balance between the analytical accuracy and the number of samples that exist within the interval. The smaller the variation range of the selected parameter is, the more accurate the analysis results are. However, if the parameter variation range is too small, the amount of data contained will be less, so that accurate statistical analyses cannot be performed. After screening the data, the scattered relationships between the wind speed and the pitch load are shown in Figure 6a–d under different rotor speeds. For Figure 6a, the hub angle is 0 rad; for Figure 6b,  $0.5\pi$  rad; for Figure 6c,  $\pi$  rad; and for Figure 6d,  $1.5\pi$  rad. As shown in Figure 6a–d, when the wind speed keeps a constant value, the pitch load changes in a certain range. Therefore, single-valued processing is employed to clearly reveal the relationship between the wind speed and the pitch load. Specifically, for a given wind speed, the corresponding probability distribution of the pitch load is constructed, and then the pitch load with the highest probability is extracted as the single-valued torque (load) corresponding to the given wind speed.

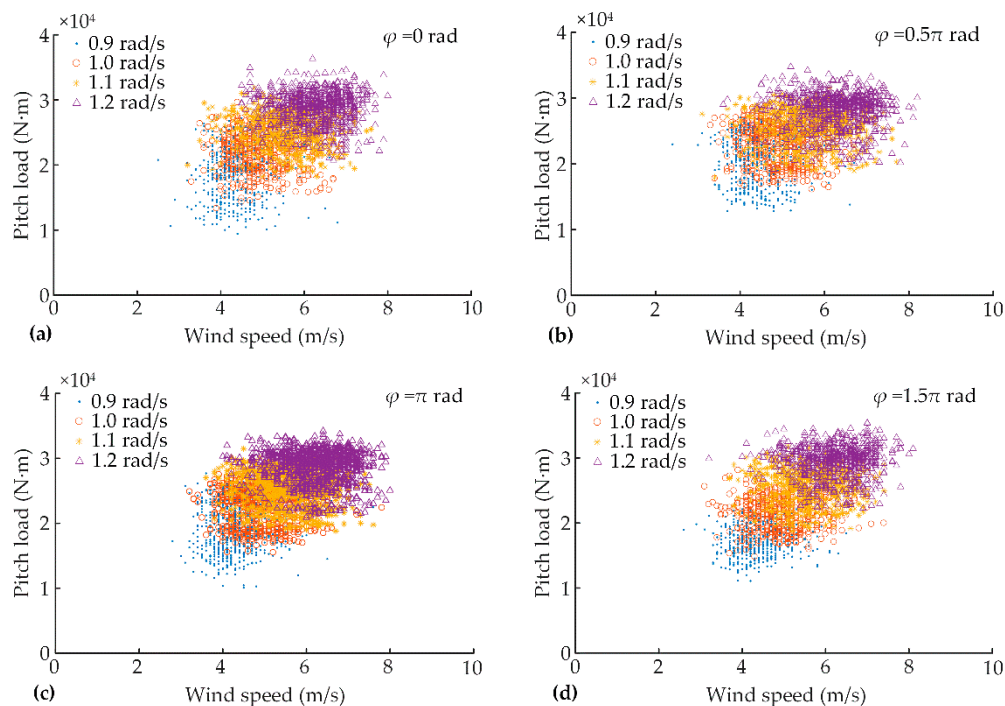


**Figure 6.** Scattered relationship between the wind speed and the pitch load: (a) The hub angle is 0 rad; (b) The hub angle is  $0.5\pi$  rad; (c) The hub angle is  $\pi$  rad; (d) The hub angle is  $1.5\pi$  rad.

In the statistical field, there are two commonly used methods to estimate the overall probability distribution density of the sample, that is, the parametric method and the nonparametric method. The parametric method considers the form of the density function to be known, and only the specific parameters of the density function are determined by the sample. However, for the blade pitch load, there is no prior knowledge about the density function. Therefore, the kernel density

estimation (KDE) [34–37], which is one kind of nonparametric density estimation method, is employed. The general definition of the KDE method is

$$\begin{cases} f_h(x) = \frac{1}{N_s h} \sum_{j=1}^{N_s} K\left(\frac{x-X_j}{h}\right) \\ K(x) \geq 0, \int_{-\infty}^{+\infty} K(x)dx = 1 \end{cases} \quad (4)$$

where  $X_j (j = 1, 2, \dots, N_s)$  is a sample of a continuous population,  $f_h(x)$  is the kernel density estimation of the total density function  $f(x)$  at any point  $x$ ,  $K(\cdot)$  is the kernel function, and  $h$  is the window width.

The common kernel functions include Uniform, Triangle, and Gauss. In this paper, the Gaussian kernel function is selected, which is [35]:

$$K(x) = \frac{1}{\sqrt{2\pi}} \exp\left(-\frac{1}{2}x^2\right) \quad (5)$$

Then, the abovementioned method is applied to data processing, as shown in Figure 5a–d, while the corresponding curves of the wind speed and the pitch load after single-valued processing are shown in Figures 7a, 7b, 7c and 7d, respectively.

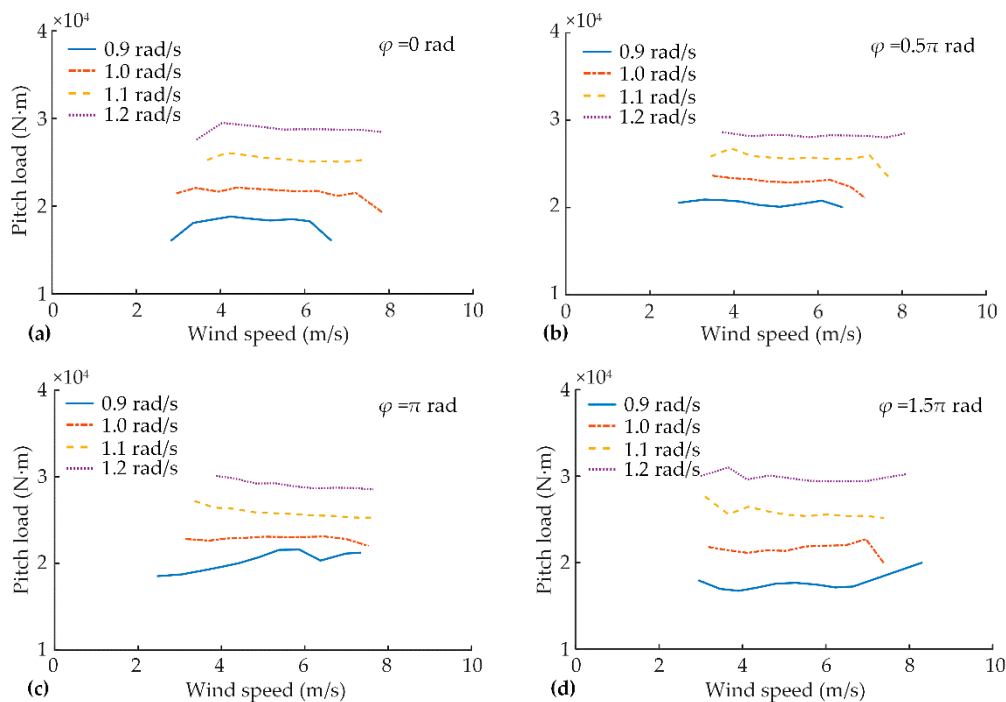


**Figure 7.** Single-valued relationship between the wind speed and the pitch load: (a) The hub angle is 0 rad; (b) The hub angle is  $0.5\pi$  rad; (c) The hub angle is  $\pi$  rad; (d) The hub angle is  $1.5\pi$  rad.

From Figures 6 and 7, it can be seen that before data processing, the relationship between wind speed and pitch load is disperse, and it is difficult to see the influence of wind speed on the pitch load. After single value processing, the relationship between the wind speed and pitch load becomes clearer. As shown in Figure 7, under a certain wind speed, the greater the rotor speed is, the larger the pitch load is. When the rotor speed is 1.2 rad/s, the corresponding pitch load is approximately 1.5 times that of the rotor speed at 0.9 rad/s. There is a noteworthy phenomenon that can be seen from Figure 6: when the rotor speed is constant, the wind speed changes within a certain range, but the change of wind speed does not cause a significant change in the pitch load. Theoretically, as the wind speed increases, the pitch load increases, especially below the rated wind speed. This trend is also evident in Figure 5. From another scenario, if the inflow wind speed is steady, a certain rotor speed corresponds

to a certain wind speed below the rated wind speed. However, due to the randomness of the wind speed and the rapidity of the wind speed change (relative to the inertia of the wind rotor), when the rotor speed is constant, the wind speed is not constant but varies within a certain range. The strong randomness of the wind speed conceals the essential relationship between the wind speed data and the pitch load. This can reasonably explain why the rotor speed corresponds to a certain range of wind speed, but the pitch load is constant.

In addition, the pitch load is not obviously kept consistent in the “two ends” of the curve in Figure 7. The reason for this phenomenon is that in the “two ends” of the curve, the amount of SCADA data that can be extracted is relatively small, and the data processing method is greatly affected by outliers, so some unreliable phenomena appear.

#### 4.2. Influence of Rotor Speed on the Pitch Load

Rotor speed can be measured accurately in the SCADA system and can be precisely controlled by the appropriate control strategy. When investigating the influence of rotor speed on the pitch load, the extraction of SCADA data mainly includes three steps to construct the subset:

*Step 1:* Eliminate the data of the wind turbine in the pitch state by judging whether  $\beta = 0$ .

*Step 2:* Select the wind speed of 4 m/s, 5 m/s, 6 m/s and 7 m/s, with a variation range of  $\pm 0.5$  m/s. The wind speed level is also determined to set aside the influence caused by the operation of the pitch mechanism.

*Step 3:* Extract the SCADA data corresponding to hub angle of 0 rad,  $0.5\pi$  rad,  $\pi$  rad and  $1.5\pi$  rad under different wind speeds, with a variation range of  $\pm 0.1$  rad.

Under the different wind speed ranges, the relationship between the rotor speed and the pitch load is obtained, as shown in Figure 8a–d. Obviously, the relationship between the rotor speed and the pitch load also has a scattered point relation, that is, a certain rotor speed corresponds to a series of pitch loads. Subsequently, the proposed KDE data processing method is used to process the relationship between the rotor speed and the pitch load in Figure 8a–d, and the corresponding single-valued relationship between the rotor speed and the pitch load is obtained as shown in Figure 9a–d.

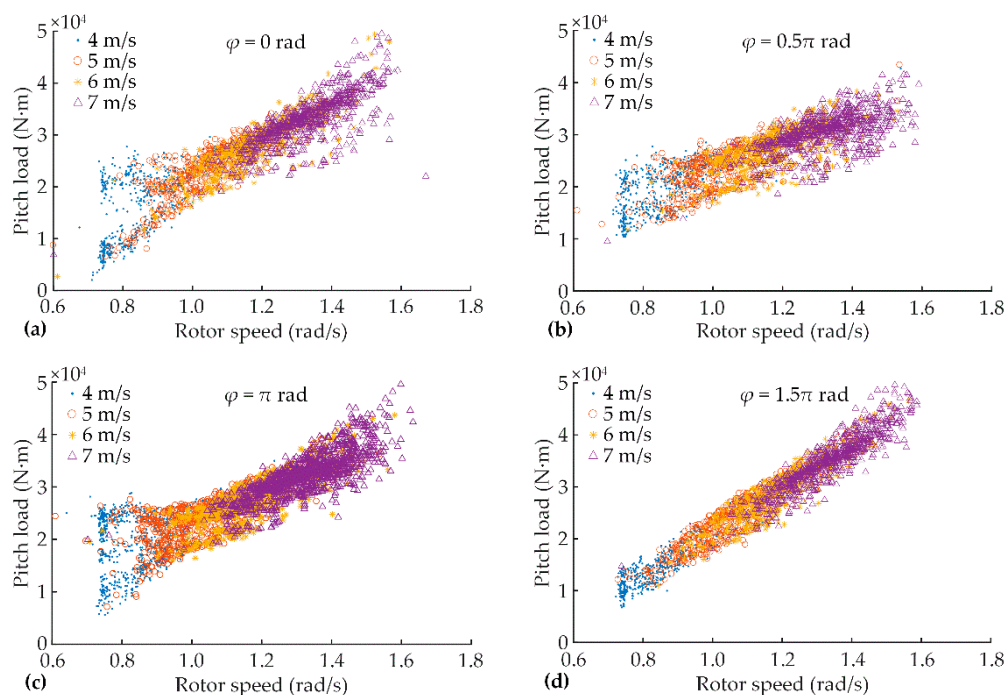


**Figure 8.** Scattered relationship between the rotor speed and the pitch load: (a) The hub angle is 0 rad; (b) The hub angle is  $0.5\pi$  rad; (c) The hub angle is  $\pi$  rad; (d) The hub angle is  $1.5\pi$  rad.

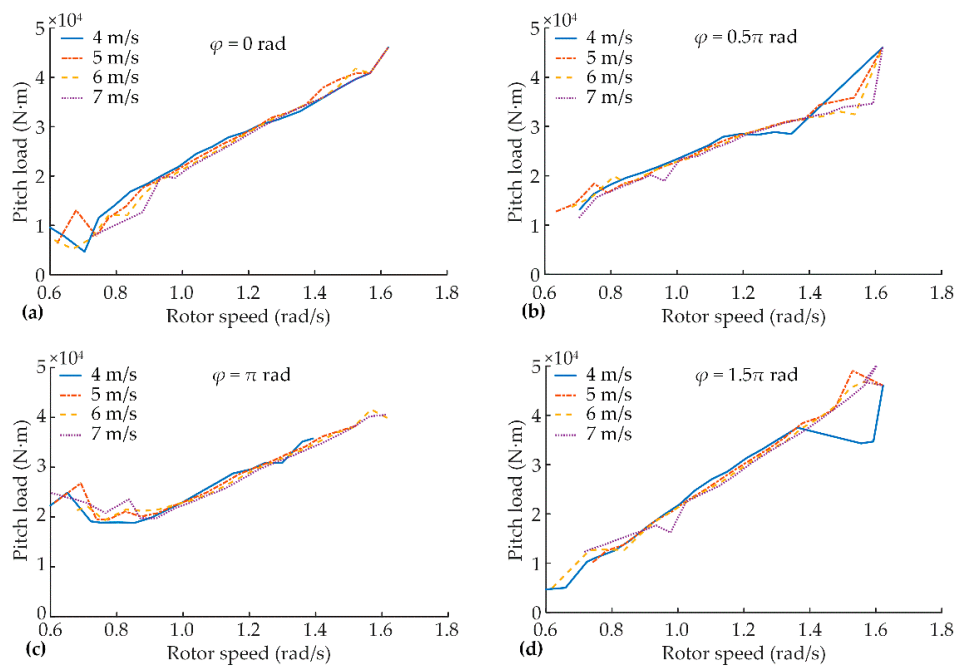


**Figure 9.** Single-valued relationship between the rotor speed and the pitch load: (a) The hub angle is 0 rad; (b) The hub angle is  $0.5\pi$  rad; (c) The hub angle is  $\pi$  rad; (d) The hub angle is  $1.5\pi$  rad.

It can be seen from Figures 8 and 9 that when the wind speed is less than the rated wind speed and the blade angle is 0 rad, the influence of the rotor speed on the pitch load is more obvious than that of the wind speed, which shows an approximately linear relationship in general. To further quantitatively analyze the relationship between the pitch load and the rotor speed, their relationship function could be considered as:

$$T_p = f(\omega) \quad (6)$$

where  $T_p$  is the pitch load; and  $\omega$  is rotor speed.

Let  $f(\omega)$  be a function with an expression of  $k\omega + b$ . Then, the least-square fittings are performed on the scattered data in Figures 8a, 8b, 8c and 8d. The fitting result between the pitch load and the rotor speed is shown in Equation (7):

$$T_p = \begin{cases} f_1(\omega) = 3.252 \times 10^4 \omega - 1.242 \times 10^4 & \varphi = 0 \\ f_2(\omega) = 2.259 \times 10^4 \omega - 701.1 & \varphi = 0.5\pi \\ f_3(\omega) = 2.524 \times 10^4 \omega - 2869 & \varphi = \pi \\ f_4(\omega) = 3.992 \times 10^4 \omega - 2.057 \times 10^4 & \varphi = 1.5\pi \end{cases} \quad (7)$$

In Equation (7), the slopes of the function between the pitch load and the rotor speed are different at different hub angles. The main reason is that at different hub angles, the wind speeds acting on the wind turbine blades are different due to the influence of wind shear. Meanwhile, the aerodynamic force that induces the pitch load is related to not only the rotor speed but also the wind speed. In addition, the fitting result also shows that the intercepts of the relational expression of the pitch load and the rotor speed vary at different hub angles. The main reason is that when the hub angle varies, not only the wind speed acting on the wind turbine blades will change due to the influence of wind shear but also the pitch load induced by the blade gravity will change.

#### 4.3. Influence of the Hub Angle on the Pitch Load

The variation in the hub angle will change the spatial position of the blade, thus affecting the pitch load induced by the blade gravity. Furthermore, the variation will also change the pitch load

induced by the aerodynamic force acting on the blades (due to the influence of wind shear). When analyzing the influence of the hub angle on the pitch load, a new data subset is grouped and mainly includes three steps:

*Step 1:* Eliminate the data of the wind turbine in the pitch state by judging whether  $\beta = 0$ .

*Step 2:* Select the wind speed of 4 m/s, 6 m/s, 8 m/s and 10 m/s, with a variation range of  $\pm 0.5$  m/s.

*Step 3:* Select the rotor speed levels from 0.8 rad/s to 1.6 rad/s, with an increase of 0.1 rad/s under different wind speeds, with a variation range of  $\pm 0.1$  rad/s.

Subsequently, the relationships between the hub angle and the pitch load are obtained under different rotor speeds, which are shown in Figure 10a–d. Obviously, there is a scatter point relationship between the hub angle and the pitch load in the figure. In other words, a hub angle value corresponds to the multiple pitch load values. By using the abovementioned KDE method, the pitch load data could be single-valued processed. The corresponding relationship between the hub angle and the pitch load is shown in Figure 11a–d.

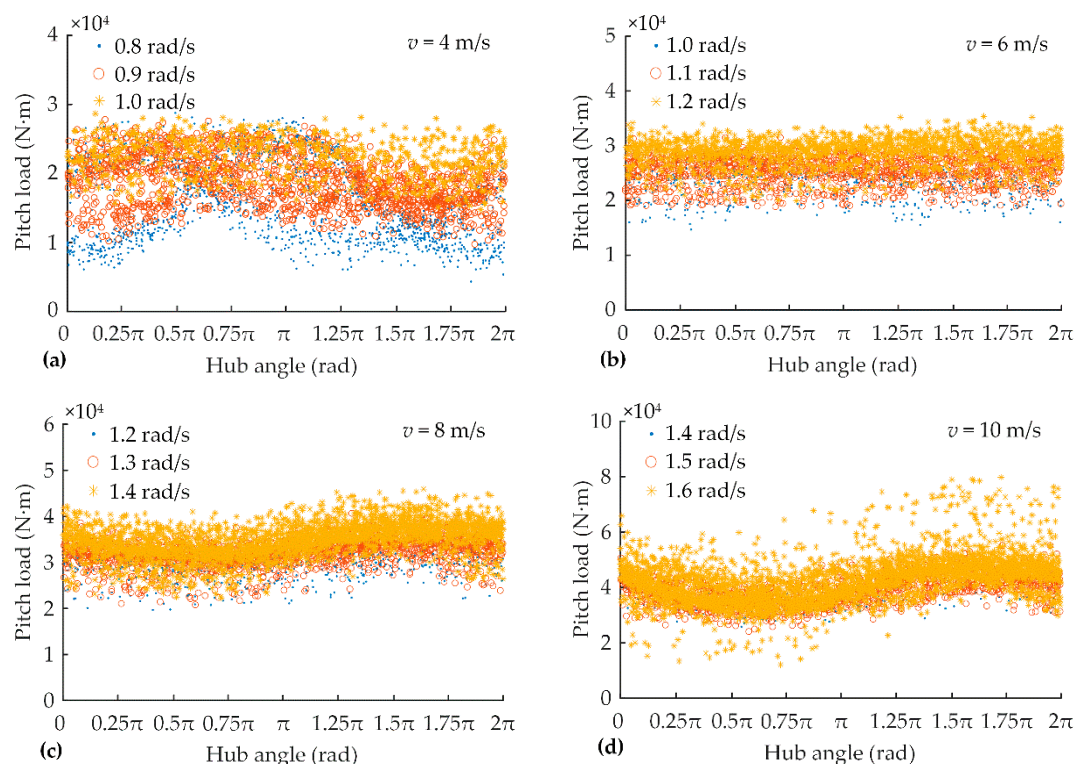


**Figure 10.** Scattered relationship between the hub angle and the pitch load: (a) The wind speed is 4 m/s; (b) The wind speed is 6 m/s; (c) The wind speed is 8 m/s; (d) The wind speed is 10 m/s.

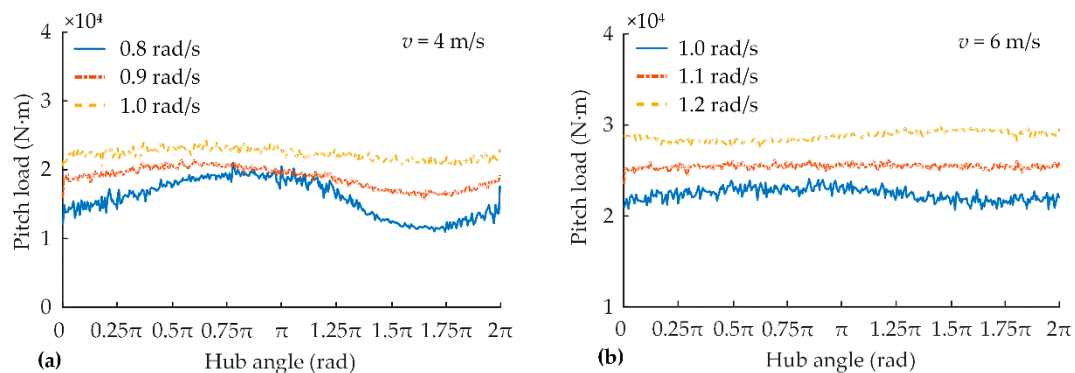


**Figure 11.** Cont.

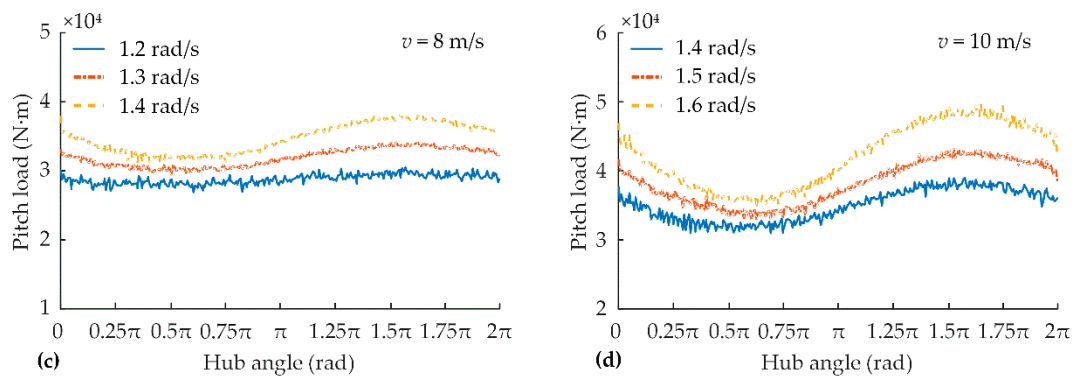


**Figure 11.** Single-valued relationship between the hub angle and the pitch load: (a) The wind speed is 4 m/s; (b) The wind speed is 6 m/s; (c) The wind speed is 8 m/s; (d) The wind speed is 10 m/s.

In Figure 11a–d, when the rotor speed and the wind speed are constant, the variation trend of the pitch load (with the change of hub angle) is approximately a sine (cosine) curve. Under the same wind speed and hub angle, the greater the rotor speed is, the greater the pitch load is. To fit the relationship between the pitch load and the hub angle in Figure 10a–d, an expression is employed as:

$$f(\varphi) = A \sin(\varphi + \varphi_0) + b \quad (8)$$

where  $f(\varphi)$  is the relationship function of the pitch load and the hub angle;  $\varphi$  is the hub angle;  $\varphi_0$  is the initial phase;  $A$  is the amplitude; and  $b$  is the offset.

Under different wind and rotor speeds, assume the pitch load samples are expressed by  $T_{p1}, T_{p2}, \dots, T_{p12}$ . The pitch load sample of  $T_{p1}$  corresponds to the wind speed  $v = 4$  m/s and rotor speed  $\omega = 0.8$  rad/s;  $T_{p12}$  corresponds to the wind speed  $v = 10$  m/s and rotor speed  $\omega = 1.6$  rad/s. For a pitch load sample from  $T_{p1}$  to  $T_{p12}$ , one has  $T_{pk} = \{T_{pj}\}$  ( $j = 1, 2, 3, \dots, N_k$ ), where  $N_k$  is the sample number contained in the  $k$ -th pitch load sample set ( $k = 1, 2, \dots, 12$ ). Then, using the least square method, the specific expression of Equation (8) could be obtained. The objective function is:

$$\begin{aligned} g(A, \varphi_0, b) &= \min \sum_{j=1}^{N_k} [T_{pj} - \hat{T}_{pj}]^2 \\ &= \min \sum_{j=1}^{N_k} \left\{ T_{pj} - [A_j \sin(\varphi + \varphi_{0j}) + b_j] \right\}^2 \end{aligned} \quad (9)$$

According to Equation (9), under different wind and rotor speeds, the values of  $A$ ,  $\varphi_0$  and  $b$  in Equation (8) can be obtained (as shown in Table 3). As seen from Table 3, with the increase in the wind and rotor speeds, amplitude  $A$  decreases first and then increases; the initial phase  $\varphi_0$  keeps decreasing; and the intercept  $b$  keeps increasing. Among the four components of pitch load (aerodynamic force, centrifugal force, gravity, inertia force), pitch load induced by the centrifugal force and pitch load induced by the inertia force are independent of the hub angle; pitch load induced by the aerodynamic force and pitch load induced by gravity are related to the hub angle. This also means that the “sine” trends of pitch load shown in Figures 10 and 11 are caused by the aerodynamic force and the blade gravity.

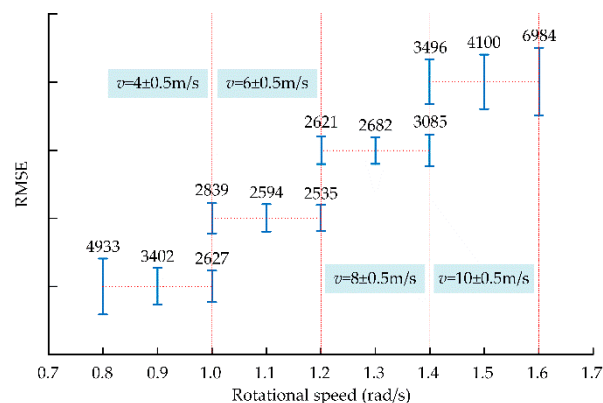
**Table 3.** The fitting result of the relation function of the pitch load and the hub angle.

Wind Speed (m/s)	Rotor Speed (rad/s)	$A$ (N·m)	$\varphi_0$ (rad)	$b$ ( $\times 10^4$ ) (N·m)	RMSE
$4 \pm 0.5$	$0.8 \pm 0.05$	3704	5.40	1.59	4933
	$0.9 \pm 0.05$	2049	5.86	1.89	3402
	$1.0 \pm 0.05$	1037	0.49	2.23	2839
$6 \pm 0.5$	$1.0 \pm 0.05$	797.5	5.41	2.24	2627
	$1.1 \pm 0.05$	143.8	4.66	2.55	2594
	$1.2 \pm 0.05$	654.8	3.20	2.87	2535
$8 \pm 0.5$	$1.2 \pm 0.05$	829.9	3.46	2.88	2621
	$1.3 \pm 0.05$	1949	3.30	3.19	2682
	$1.4 \pm 0.05$	3026	3.22	3.48	3085
$10 \pm 0.5$	$1.4 \pm 0.05$	3339	3.40	3.53	3496
	$1.5 \pm 0.05$	4435	3.57	3.85	4100
	$1.6 \pm 0.05$	6555	2.81	4.24	6984

Since the magnitude and phase of sinusoidal changes of the pitch load induced by the gravity component are all determinable, it can be deduced that the phenomenon of amplitude  $A$  decreasing first and then increasing, as shown in Table 3, is caused by the change in the aerodynamic force component. In other words, the initial phase of the pitch load induced by the aerodynamic force is various at different wind and rotor speeds, which leads to the phenomenon that amplitude  $A$  decreases first and then increases, and the initial phase  $\varphi_0$  keeps decreasing after the superposition of various pitch load components. In addition, amplitude  $A$  reflects the fluctuation of the pitch load during the maximum wind energy capture stage. It can be seen in Table 3 that the maximum value of  $A$  is 6555 N·m, which means the maximum fluctuation of pitch load is  $2 \times A = 1.311 \times 10^4$  N·m.

Since the SCADA data with constant pitch angle were selected, the influence of the inertia load on the fitting results can be excluded. During the rotation of the rotor, the centrifugal force of the blade is always along the extension direction of the blade. Therefore, the pitch loads induced by centrifugal force are not influenced by the change of the hub angle but are only related to the rotor speed. Therefore, the change in the centrifugal force will not affect parameters  $A$  and  $\varphi_0$  in Table 3, but only affect the change of intercept  $b$ . It can also be seen from Table 3 that intercept  $b$  is increasing with the increase of the rotor speed. This means the greater the rotor speed is, the greater the pitch load induced by centrifugal force is.

When realizing Equation (8) by using the least square method, the variation trend of the fitting root-mean-square error (RMSE) with the change of the wind and rotor speeds are shown in Figure 12.

**Figure 12.** RMSE calculation result.

In Figure 12, the length of the line segment is used to describe the size of the fitting root-mean-square error. The fitting root-mean-square error reflects the deviation of the relation curve (between the hub angle and the pitch load) with respect to the sine function described in Equation (8). In other words, the larger the fitting root-mean-square error is, the greater the deviation is. The fitting root-mean-square error also reflects the comprehensive composition relation of the pitch load induced by aerodynamic force, the pitch load induced by the centrifugal force and the pitch load induced by the blade gravity. As seen from Figure 12, under a certain rotor speed, the greater the wind speed is, the greater the fitting root-mean-square error is. Since the pitch load induced by centrifugal force stays unchanged and the “sine” change of the pitch load induced by the blade gravity are not affected by the rotor speed, it can be understood that the greater the wind speed is, the more dispersed the pitch load induced by the aerodynamic force is.

#### 4.4. The Influence of Pitch Angle on the Pitch Load

To control the wind energy capture, wind turbines could control the pitch angle, which also changes the load acting on the blade. Theoretically, when the wind speed is lower than the rated wind speed, the pitch mechanism is fixed, and the pitch angle is 0 rad. During this period, the wind turbine runs at the maximum wind energy capture stage by maintaining the optimal tip speed ratio through controlling the rotor speed. When the wind speed is higher than the rated wind speed, the wind turbine starts the pitch mechanism and controls the pitch angle to adapt to the change in wind speed, so that the output power keeps at the rated power level, which is called the constant power operation stage. However, in practice, the start-up of the pitch mechanism is determined by the power of the wind turbine, not the wind speed. Although the wind speed sometimes does not reach the rated wind speed, the pitch mechanism still may have been started.

During the operating of the pitch mechanism, there are two operating states, that is, the increase of the pitch angle and the decrease of the pitch angle. This means that even at the same pitch angle, the wind turbine may be running at different operating states, and the load characteristics may be different under different conditions. To this end, the pitch rate is defined to determine the state of the pitch mechanism. That is:

$$\eta(t) = \frac{\beta(t+T) - \beta(t)}{T} \quad (10)$$

where,  $\beta(t)$  is the corresponding pitch angle at time  $t$ ; and  $T$  is the data sampling period of the SCADA system.

Considering the fluctuation of the pitch angle in the process of varying pitch, the pitch rate is modified as:

$$\Gamma(t) = \eta(t-2) \cdot \eta(t-1) \cdot \eta(t) \quad (11)$$

When  $\Gamma(t)$  satisfies  $\Gamma(t) > 0$  in Equation (11), the pitch load is considered to be SCADA data with a continuously increasing pitch angle. When  $\Gamma(t) < 0$  is satisfied, the pitch load is considered to be a SCADA data with a continuously decreasing pitch angle. When  $\Gamma(t) = 0$  is satisfied, the pitch load is considered to be SCADA data with a constant pitch angle. Therefore, the data set distribution illustrated in Figure 5 is transformed into that which is illustrated in Figure 13. It can be seen from Figure 13 that the data samples with wind speeds greater than 8 m/s correspond to three types: (1) data with a constant pitch angle, which is defined as non-pitch; (2) data during the increase of the pitch angle, which is defined as increasing pitch; (3) data during the decrease of the pitch angle, which is defined as the decreasing pitch. Considering there are more data samples distributed near the rated wind speed, a subset of data samples with a wind speed of 11 m/s and a rotor speed of 1.78 rad/s is extracted, and then four subsets of the rotor angles of 0 rad,  $0.5\pi$  rad,  $\pi$  rad, and  $1.5\pi$  rad are divided from the subset to analyze the influences of pitch angle to the pitch load.

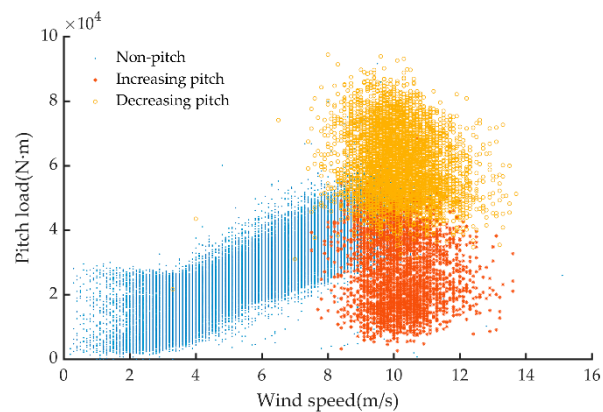


**Figure 13.** Scattered relationship between the wind speed and pitch load under different states.

The relationships between the pitch angle and the pitch load are plotted in Figures 14a, 14b, 14c and 14d, which correspond to the hub angles of 0 rad,  $0.5\pi$  rad,  $\pi$  rad, and  $1.5\pi$  rad, respectively.

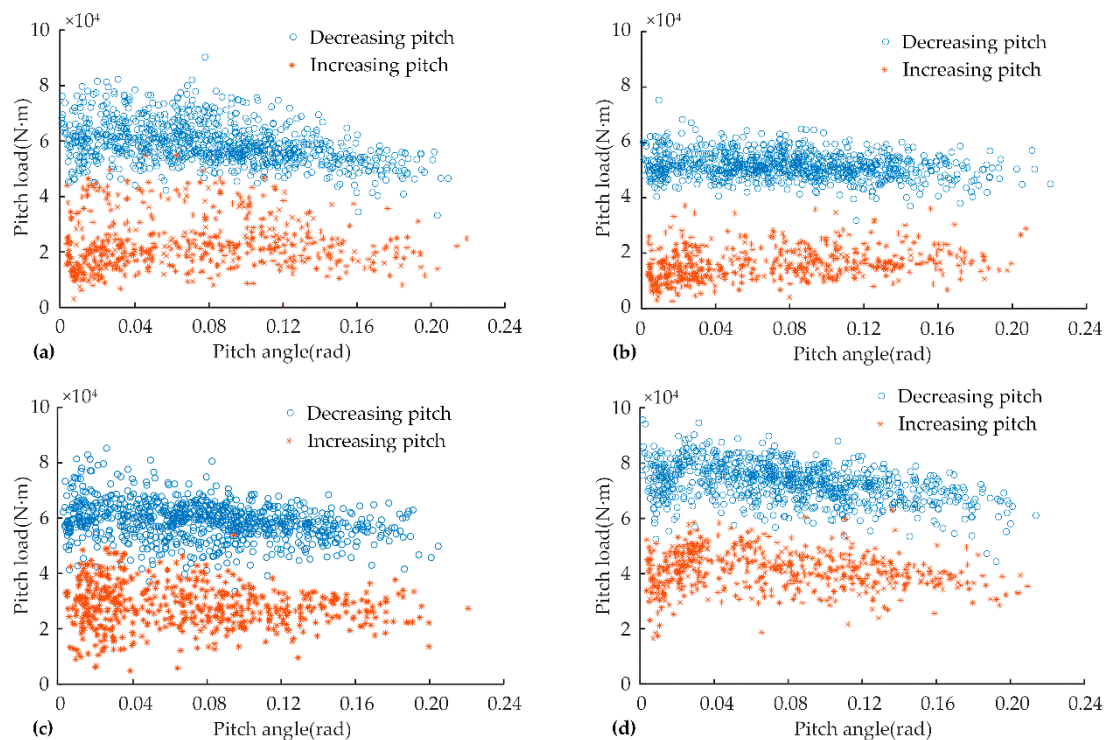


**Figure 14.** Scattered relationship between the pitch angle and the pitch load: (a) The hub angle is 0 rad; (b) The hub angle is  $0.5\pi$  rad; (c) The hub angle is  $\pi$  rad; (d) The hub angle is  $1.5\pi$  rad.

Obviously, there is a scattered multivalued relation between the pitch angle and the pitch load. Using the abovementioned KDE method, the data are processed to obtain the single-valued relation between the pitch angle and pitch load. The results are shown in Figures 15a, 15b, 15c and 15d, respectively.

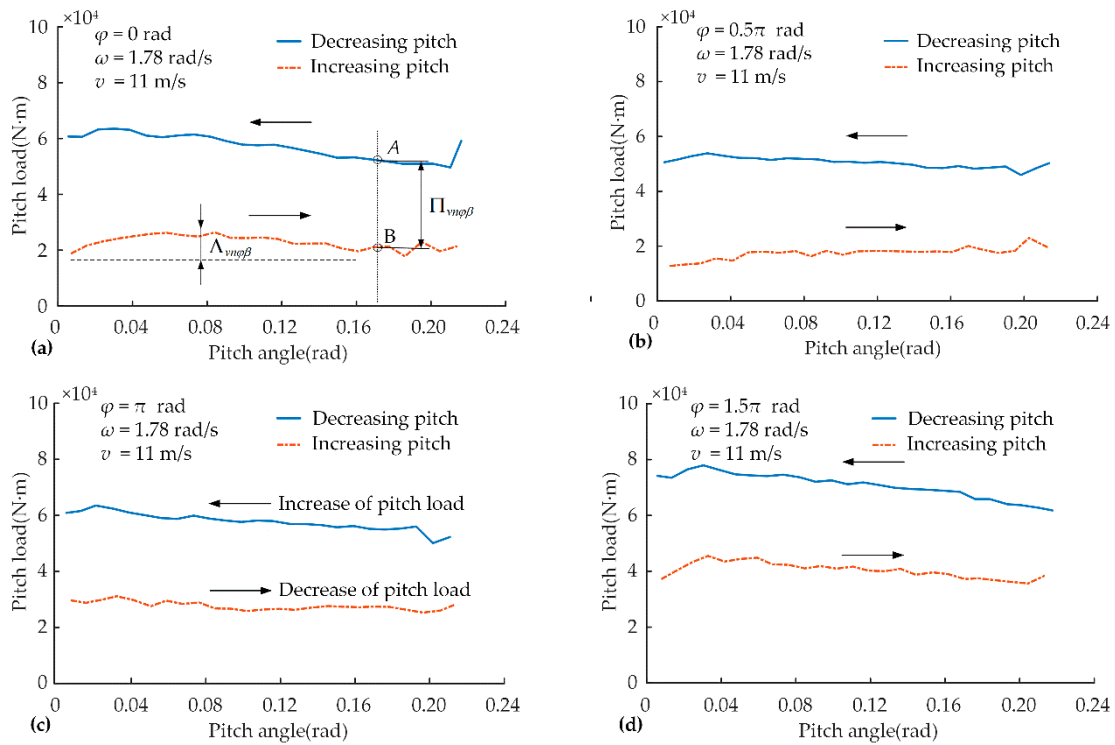


**Figure 15.** Single-valued relationship between the pitch angle and the pitch load: (a) The hub angle is 0 rad; (b) The hub angle is  $0.5\pi$  rad; (c) The hub angle is  $\pi$  rad; (d) The hub angle is  $1.5\pi$  rad.

Figures 14 and 15 show that under constant wind and rotor speeds, the pitch load generally declines in the increasing pitch status and gradually increases in the decreasing pitch status. From Figure 15a to Figure 15d, it is clear that under the same wind speed, rotor speed and hub angle, the pitch load in the increasing pitch status is significantly less than that in the decreasing pitch status. The load fluctuation  $\Delta_{vn\phi\beta}$  marked in Figure 15a reflects the comprehensive influence of three pitch load components; that is, the aerodynamic-force-induced pitch load, the centrifugal-force-induced pitch load and the gravity-induced pitch load. For points A and B in Figure 15a, they have the same pitch angle, which means that the pitch load components that are induced by gravity are the same. Meanwhile, the pitch load components induced by the centrifugal force are also the same due to the same rotor speed. Thus, the differences in the pitch load (denoted by  $\Pi_{vn\phi\beta}$ ) between points A and B are caused by the difference of the pitch load induced by aerodynamic force. This also illustrates that in the increasing pitch status, the aerodynamic force will push the blade rotation as a motive force. In the decreasing pitch status, the aerodynamic force will block the blade rotation in resistance. Furthermore, under different hub angles, the effects of this kind of “push” or “block” are different.

To quantitatively describe the different  $\Pi_{vn\phi\beta}$  of the pitch load induced by the aerodynamic force in the process of variable pitch, a difference index of the pitch load is proposed. Assuming that under different hub angles, the pitch load dataset with decreasing pitch status is  $T_{vn\phi}$ , while the pitch load data set is  $T'_{vn\phi}$  with increasing pitch status. Then,  $T_{vn\phi} = \{T_{vn\phi 1}, T_{vn\phi 2}, \dots, T_{vn\phi l}\}$ ,  $T'_{vn\phi} = \{T'_{vn\phi 1}, T'_{vn\phi 2}, \dots, T'_{vn\phi l}\}$ , and ( $l = 1, 2, 3, \dots, N_{vn\phi}$ ); where  $N_{vn\phi}$  is the sample number of the pitch load dataset when the wind speed is  $v$ , the rotor speed is  $\omega$ , and the hub angle is  $\phi$ . The “difference index” is to be expressed as:

$$\Pi_{vn\phi} = \frac{1}{N_{vn\phi}} \sum_{l=1}^{N_{vn\phi}} [T_{vn\phi l} - T'_{vn\phi l}] \tag{12}$$

where  $\Pi_{v\omega\varphi}$  denotes the “difference index” between the pitch load in the decreasing pitch status and the pitch load in the increasing pitch status under the condition that the wind speed is  $v$ , the rotor speed is  $\omega$  and the hub angle is  $\varphi$ .

According to Equation (12), and under the condition that wind speed is  $v = 11$  m/s and the rotor speed is  $\omega = 1.78$  rad/s, the difference indexes are  $\Pi_1 = 3.40 \times 10^4$  N · m,  $\Pi_2 = 3.21 \times 10^4$  N · m,  $\Pi_3 = 3.01 \times 10^4$  N · m, and  $\Pi_4 = 3.00 \times 10^4$  N · m corresponding to the hub angles of 0 rad,  $0.5\pi$  rad,  $\pi$  rad and  $1.5\pi$  rad, respectively. The calculation results show that the difference indexes under different hub angles are small. It also reflects the variation amplitude of the pitch load during the working process of the pitch system. Compared with the maximum wind energy capture stage discussed earlier, the maximum load and variable amplitude of the variable propeller load of the wind turbine in the constant power operation stage was much larger. It was required to pay sufficient attention to the design and maintenance of the pitch mechanism of the wind turbine.

## 5. Conclusions

For a long time, the understanding of the pitch load was not clear enough. According to the investigation of the pitch load in this paper, the basic characteristics and mechanism of pitch load can be further understood. Additionally, this study can provide the basis for the investigation of the wind turbine accidents. Moreover, it can provide a basis for wind turbine maintenance, especially for the pitch system. Some specific conclusions are summarized as follows.

Due to the randomness of wind speed and the rapidity of wind speed change, when the rotor speed is constant, the wind speed is not constant but varies within a certain range. The strong randomness of wind speed conceals the essential relationship between the wind speed data and the pitch load. Under the rated wind speed, the pitch load increases with the rotor speed increase, and there is an approximate linear relationship between the rotor speed and the pitch load.

The relationship between the hub angle and the pitch load is a similar sine (cosine) law. This is caused by the influence of aerodynamic force and gravity that occurs among the four components of the pitch load (aerodynamic force, centrifugal force, gravity, inertia force). The change in the aerodynamic force affects the amplitude and phase of the sine (cosine) curve. The change in the centrifugal force affects its intercept.

Due to the influence of wind speed randomness and wind rotor inertia force during the actual operation of the wind turbine, when the wind speed does not reach the rated wind speed, the pitch mechanism of the wind turbine may have been started. Under a certain wind speed and rotor rotational speed, the pitch load decreases during the increasing pitch status and increases gradually during the decreasing pitch status. Compared with the maximum wind energy capture stage, the maximum load and load variation range of the pitch mechanism are much larger when the wind turbine is running at the constant power stage, which requires sufficient attention in the design and maintenance of the wind turbine.

**Author Contributions:** The research presented in this paper was a collaborative effort among all authors. Conceptualization, F.Z. and J.D.; Methodology, F.Z. and J.D.; Visualization, L.L.; Writing—original draft, F.Z.; Writing—review & editing, J.D., D.L. and X.L.

**Funding:** This research was funded by National Natural Science Foundation of People’s Republic of China (grant number 51475160, 51675175), Hunan Provincial Natural Science Foundation (grant number 2016JJ5024).

**Conflicts of Interest:** The authors declare no conflicts of interest.

## References

1. GWEC. *Global Wind Report: Annual Market Update 2017*; GWEC: Brussels, Belgium, 2017.
2. Dai, J.; Yang, X.; Wen, L. Development of wind power industry in China: A comprehensive assessment. *Renew. Sustain. Energy Rev.* **2018**, *97*, 156–164. [[CrossRef](#)]
3. Yang, C.; Qian, Z.; Pei, Y.; Wei, L. A Data-Driven Approach for Condition Monitoring of Wind Turbine Pitch Systems. *Energies* **2018**, *11*, 2142. [[CrossRef](#)]

4. Barnes, R.H.; Morozov, E.V. Structural optimisation of composite wind turbine blade structures with variations of internal geometry configuration. *Compos. Struct.* **2016**, *152*, 158–167. [[CrossRef](#)]
5. Rosemeier, M.; Berring, P.; Branner, K. Non-linear ultimate strength and stability limit state analysis of a wind turbine blade. *Wind Energy* **2016**, *19*, 825–846. [[CrossRef](#)]
6. Amirat, Y.; Benbouzid, M.E.H.; Al-Ahmar, E.; Bensaker, B.; Turri, S. A brief status on condition monitoring and fault diagnosis in wind energy conversion systems. *Renew. Sustain. Energy Rev.* **2009**, *13*, 2629–2636. [[CrossRef](#)]
7. Liu, W.; Zhang, W.; Han, J.; Wang, G. A new wind turbine fault diagnosis method based on the local mean decomposition. *Renew. Energy* **2012**, *48*, 411–415. [[CrossRef](#)]
8. Kabir, I.F.S.A.; Ng, E. Insight into stall delay and computation of 3D sectional aerofoil characteristics of NREL phase VI wind turbine using inverse BEM and improvement in BEM analysis accounting for stall delay effect. *Energy* **2017**, *120*, 518–536. [[CrossRef](#)]
9. Prajapat, G.P.; Senroy, N.; Kar, I.N. Wind turbine structural modeling consideration for dynamic studies of DFIG based system. *IEEE Trans. Sustain. Energy* **2017**, *8*, 1463–1472. [[CrossRef](#)]
10. Tahani, M.; Kavari, G.; Masdari, M.; Mirhosseini, M. Aerodynamic design of horizontal axis wind turbine with innovative local linearization of chord and twist distributions. *Energy* **2017**, *131*, 78–91. [[CrossRef](#)]
11. Elgammi, M.; Sant, T. A new stall delay algorithm for predicting the aerodynamics loads on wind turbine blades for axial and yawed conditions. *Wind Energy* **2017**, *20*, 1645–1663. [[CrossRef](#)]
12. Hand, B.; Cashman, A.; Kelly, G. A low-order model for offshore floating vertical axis wind turbine aerodynamics. *IEEE Trans. Ind. Appl.* **2017**, *53*, 512–520. [[CrossRef](#)]
13. Li, Y.; Castro, A.; Martin, J.; Sinokrot, T.; Prescott, W.; Carrica, P. Coupled computational fluid dynamics/multibody dynamics method for wind turbine aero-servo-elastic simulation including drivetrain dynamics. *Renew. Energy* **2017**, *101*, 1037–1051. [[CrossRef](#)]
14. Marten, D.; Bianchini, A.; Pechlivanoglou, G.; Balduzzi, F.; Nayeri, C.N.; Ferrara, G.; Paschereit, C.O.; Ferrari, L. Effects of Airfoil's Polar Data in the Stall Region on the Estimation of Darrieus Wind Turbine Performance. *J. Eng. Gas Turbines Power* **2016**, *139*, 022606:1–022606:9. [[CrossRef](#)]
15. Meyer Forsting, A.R.; Troldborg, N.; Murcia Leon, J.P.; Sathe, A.; Angelou, N.; Vignaroli, A. Validation of a CFD model with a synchronized triple-lidar system in the wind turbine induction zone. *Wind Energy* **2017**, *20*, 1481–1498. [[CrossRef](#)]
16. Najafian Ashrafi, Z.; Ghaderi, M.; Sedaghat, A. Parametric study on off-design aerodynamic performance of a horizontal axis wind turbine blade and proposed pitch control. *Energy Convers. Manag.* **2015**, *93*, 349–356. [[CrossRef](#)]
17. Wang, T.; Wang, L.; Zhong, W.; Xu, B.; Chen, L. Large-scale wind turbine blade design and aerodynamic analysis. *Chin. Sci. Bull.* **2012**, *57*, 466–472. [[CrossRef](#)]
18. Dai, J.; Hu, Y.; Liu, D.; Long, X. Calculation and characteristics analysis of blade pitch loads for large scale wind turbines. *Sci. China Technol. Sci.* **2010**, *53*, 1356–1363. [[CrossRef](#)]
19. Dai, J.C.; Hu, Y.P.; Liu, D.S.; Long, X. Aerodynamic loads calculation and analysis for large scale wind turbine based on combining BEM modified theory with dynamic stall model. *Renew. Energy* **2011**, *36*, 1095–1104. [[CrossRef](#)]
20. Dai, J.C.; Hu, Y.P.; Liu, D.S.; Wei, J. Modelling and analysis of direct-driven permanent magnet synchronous generator wind turbine based on wind-rotor neural network model. *Proc. Inst. Mech. Eng. Part A* **2011**, *226*, 62–72. [[CrossRef](#)]
21. Dai, J.; Hu, W.; Shen, X. Load and dynamic characteristic analysis of wind turbine flexible blades. *J. Mech. Sci. Technol.* **2017**, *31*, 1569–1580. [[CrossRef](#)]
22. Bashirzadeh Tabrizi, A.; Whale, J.; Lyons, T.; Urmee, T.; Peinke, J. Modelling the structural loading of a small wind turbine at a highly turbulent site via modifications to the Kaimal turbulence spectra. *Renew. Energy* **2017**, *105*, 288–300. [[CrossRef](#)]
23. Hur, S.; Recalde-Camacho, L.; Leithead, W.E. Detection and compensation of anomalous conditions in a wind turbine. *Energy* **2017**, *124*, 74–86. [[CrossRef](#)]
24. Borchersen, A.B.; Kinnaert, M. Model-based fault detection for generator cooling system in wind turbines using SCADA data. *Wind Energy* **2015**, *19*, 593–606. [[CrossRef](#)]

25. Leahy, K.; Gallagher, C.; O'Donovan, P.; Bruton, K.; O'Sullivan, T.D. A Robust Prescriptive Framework and Performance Metric for Diagnosing and Predicting Wind Turbine Faults Based on SCADA and Alarms Data with Case Study. *Energies* **2018**, *11*, 1738. [[CrossRef](#)]
26. Sun, P.; Li, J.; Wang, C.; Lei, X. A generalized model for wind turbine anomaly identification based on SCADA data. *Appl. Energy* **2016**, *168*, 550–567. [[CrossRef](#)]
27. Yang, W.; Tavner, P.J.; Crabtree, C.J.; Feng, Y.; Qiu, Y. Wind turbine condition monitoring: Technical and commercial challenges. *Wind Energy* **2012**, *17*, 673–693. [[CrossRef](#)]
28. Dai, J.; Cao, J.; Liu, D.; Wen, L.; Long, X. Power fluctuation evaluation of large-scale wind turbines based on SCADA data. *IET Renew. Power Gen.* **2017**, *11*, 395–402. [[CrossRef](#)]
29. Francesco, C.; Davide, A.; Matteo, M.; Massimiliano, B.; Cathérine, M.; Emanuele, P. Wind Power Forecasting techniques in complex terrain: ANN vs. ANN-CFD hybrid approach. *J. Phys. Conf. Ser.* **2016**, *753*, 082002.
30. Saleh, A.E.; Moustafa, M.S.; Abo-Al-Ez, K.M.; Abdullah, A.A. A hybrid neuro-fuzzy power prediction system for wind energy generation. *Int. J. Electr. Power Energy Syst.* **2016**, *74*, 384–395. [[CrossRef](#)]
31. Dai, J.; Tan, Y.; Yang, W.; Wen, L.; Shen, X. Investigation of wind resource characteristics in mountain wind farm using multiple-unit SCADA data in Chenzhou: A case study. *Energy Convers. Manag.* **2017**, *148*, 378–393. [[CrossRef](#)]
32. Dai, J.; Liu, D.; Wen, L.; Long, X. Research on power coefficient of wind turbines based on SCADA data. *Renew. Energy* **2016**, *86*, 206–215. [[CrossRef](#)]
33. Dai, J.C. Dynamic Characteristics Analyzed of Large Scale Directly-driven Wind Turbines under Blade Fracture Accident Condition. *J. Mech. Eng.* **2013**, *49*, 7. [[CrossRef](#)]
34. Bessa, R.J.; Miranda, V.; Botterud, A.; Wang, J.; Constantinescu, E.M. Time Adaptive Conditional Kernel Density Estimation for Wind Power Forecasting. *IEEE Trans. Sustain. Energy* **2012**, *3*, 660–669. [[CrossRef](#)]
35. Burton, T.; Sharpe, D.; Jenkins, N.; Bossanyi, E. *Wind Energy Handbook*; John Wiley & Sons Ltd.: Hoboken, NJ, USA, 2005. [[CrossRef](#)]
36. Lakshmanan, K.; Ortner, R.; Ryabko, D. Improved Regret Bounds for Undiscounted Continuous Reinforcement Learning. In Proceedings of the 32nd International Conference on Machine Learning, Lille, France, 6–11 July 2015; pp. 524–532.
37. Liu, Z.; Shi, R.; Shen, L.; Xue, Y.; Ngan, K.N.; Zhang, Z. Unsupervised Salient Object Segmentation Based on Kernel Density Estimation and Two-Phase Graph Cut. *IEEE Trans. Multimedia* **2012**, *14*, 1275–1289. [[CrossRef](#)]



© 2019 by the authors. Licensee MDPI, Basel, Switzerland. This article is an open access article distributed under the terms and conditions of the Creative Commons Attribution (CC BY) license (<http://creativecommons.org/licenses/by/4.0/>).